Published in final edited form as:
Calcif Tissue Int. 2008 November ; 83(5): 342–353. doi:10.1007/s00223-008-9176-8.

Fourier Transform Infrared Imaging Microspectroscopy and Tissue-Level Mechanical Testing Reveal Intraspecies Variation in Mouse Bone Mineral and Matrix Composition

Hayden-William Courtland,
Division of Endocrinology, Diabetes, and Bone Diseases, Mount Sinai School of Medicine, New York, NY, USA, e-mail: hayden-william.courtland@mssm.edu

Philip Nasser,
Leni & Peter W. May Department of Orthopedics, Mount Sinai School of Medicine, Box 1188, One Gustave Levy Place, New York, NY 10029, USA, e-mail: philip.nasser@mssm.edu

Andrew B. Goldstone,
Leni & Peter W. May Department of Orthopedics, Mount Sinai School of Medicine, Box 1188, One Gustave Levy Place, New York, NY 10029, USA, e-mail: andrew.goldstone@mssm.edu

Lyudmila Spevak,
Musculoskeletal Integrity Program, Hospital for Special Surgery, New York, NY, USA, e-mail: spevakm@hss.edu

Adele L. Boskey, and
Musculoskeletal Integrity Program, Hospital for Special Surgery, New York, NY, USA, e-mail: boskeya@hss.edu

Karl J. Jepsen
Leni & Peter W. May Department of Orthopedics, Mount Sinai School of Medicine, Box 1188, One Gustave Levy Place, New York, NY 10029, USA

Abstract

Fracture susceptibility is heritable and dependent upon bone morphology and quality. However, studies of bone quality are typically overshadowed by emphasis on bone geometry and bone mineral density. Given that differences in mineral and matrix composition exist in a variety of species, we hypothesized that genetic variation in bone quality and tissue-level mechanical properties would also exist within species. Sixteen-week-old female A/J, C57BL/6J (B6), and C3H/HeJ (C3H) inbred mouse femora were analyzed using Fourier transform infrared imaging and tissue-level mechanical testing for variation in mineral composition, mineral maturity, collagen cross-link ratio, and tissue-level mechanical properties. A/J femora had an increased mineral-to-matrix ratio compared to B6. The C3H mineral-to-matrix ratio was intermediate of A/J and B6. C3H femora had reduced acid phosphate and carbonate levels and an increased collagen cross-link ratio compared to A/J and B6. Modulus values paralleled mineral-to-matrix values, with A/J femora being the most stiff, B6 being the least stiff, and C3H having intermediate stiffness. In addition, work-to-failure varied among the strains, with the highly mineralized and brittle A/J femora performing the least amount of work-to-failure. Inbred mice are therefore able to differentially modulate the composition of their bone mineral and the maturity of their bone matrix in conjunction with tissue-level mechanical properties. These results suggest that specific combinations of bone quality and morphological traits are genetically regulated such that mechanically functional bones can be constructed in different ways.

e-mail: karl.jepsen@mssm.edu.

Keywords

Bone fracture; Genetics; Mechanical property; Tissue quality; Fourier transform infrared; Mouse

Fragility fractures affect both young adults (i.e., stress fractures) and the elderly (i.e., osteoporosis). In an attempt to determine the structural basis for fracture susceptibility, studies have revealed that morphology (size and shape) [1-3] as well as quality (composition, microstructure) [4-7] can affect bone mechanical properties. However, much of this research has focused on the composite parameter bone mineral density (BMD) [8-10]. Despite heavy reliance on BMD, researchers and clinicians often note that more subtle variation at the ultrastructural level may influence bone functionality [7,11,12], yet this theory has received relatively little investigation.

Groundbreaking work indicating that mineral and matrix variation influences bone functionality comes from interspecies studies by Currey and others. It was observed that very small changes (<5%) in the percent weight of mineral resulted in 10-fold changes in stiffness and strength [13-18]. Similarly, studies have reported that variation in collagen orientation [19,20] and collagen cross-linking [21,22] are associated with altered bone stiffness and strength. Such major differences in bone mineral and matrix deposition are observed across species in both similar (i.e., human and alligator femora) and different (i.e., whale bulla and deer antler) bone structures. This interspecies variation suggests that genetic background plays a role in directing bone cells to build different types of bone tissue in order to satisfy mechanical functionality. If genetic variation can result in significant alterations in bone quality across species, it stands to reason that natural genetic variation within a species may give rise to differences in tissue deposition or maturity and play a significant role in determining bone functionality for individuals [23].

At the macroscopic level, intraspecies genetic regulation of bone functionality is clearly established in fracture risk. Both BMD, a successful tool for predicting fracture risk in a clinical setting [10], and an individual's personal or family history of fracture [24-26] show strong correlations with fracture susceptibility and are able to assist in explaining why one individual may be at risk for fracture while another is not. Research in our laboratory further clarified the importance of intraspecies genetic variation in bone functionality by using inbred mice. It was shown that intraspecies genetic variation is accompanied by statistically significant differences in whole-bone mineral content (<5% difference in ash weight percentage of mineral among strains) [27,28] and tissue mineral density (TMD) as measured by micro-computed tomography (micro-CT) [29]. In addition, mineral covaried with morphological traits such that differing sets of traits defined whole-bone mechanical properties [2,29]. Thus, different genetic backgrounds are known to give rise to sets of traits that covary to maintain bone functionality. However, the extent and importance of mineral and matrix variation at the tissue level remains unclear.

Given that intraspecies variation in murine whole-bone mineral content and mechanical properties appears to mirror interspecies variation, we hypothesized that tissue-level differences in the mineral content, mineral composition, mineral maturity, and matrix maturity would exist among murine bones with different genetic backgrounds. In addition, we expected tissue-level bone mechanical properties to vary among inbred mice. To test these hypotheses, we used Fourier transform infrared imaging (FTIRI) and a custom tissue-level mechanical testing system to relate mineral and matrix variation to tissue-level mechanical properties in three inbred mouse strains with known differences in whole-bone morphology, quality, and mechanical properties.

Materials and Methods

Animals

A total of 52 female A/J, C57BL/6J (B6), and C3H/HeJ (C3H) mice were purchased from Jackson Laboratory (Bar Harbor, ME, USA) at 8 weeks of age and housed at the animal care facility of the Mount Sinai School of Medicine on a 12-hour light:dark cycle. Mice were fed a standard feed (Purina Laboratory Chow 5001; Purina Mills, St. Louis, MO, USA) and water ad libitum. At 16 weeks of age mice were killed and the femora removed. Analyses were performed on 16-week-old mice because at this age the rate of bone growth is minimal [2, 30]. Further, mineralization data show that interstrain differences are clearly established by 16 weeks and the differences remain through 1 year [2]. The Mount Sinai Institutional Animal Care and Use Committee approved all procedures for the treatment of mice.

Compositional Traits

Right femora from A/J (n = 6), B6 (n = 7), and C3H (n = 8) mice were isolated, cleaned, embedded in polymethylmethacrylate (PMMA) [27], sectioned (coronal, 2 μm thick) using the RM2165 rotary microtome (Leica Microsystems, Exton, PA, USA), and mounted on 25 × 2 mm barium fluoride infrared windows (Spectral Systems, Hopewell Junction, NY, USA) for FTIRI. Two to three replicate sections were taken from each animal. Each section was analyzed using a Perkin-Elmer Spotlight Imaging System (Waltham, MA, USA) Spotlight Imaging System. The spectral resolution was 4 cm^{-1}, and regions of approximately 25 × 500 μm were analyzed at 6.25 μm pixel size in transmittance mode. Each image was taken at the mid-diaphysis of the anterior-medial cortex below the third trochanter. This region was chosen for analysis because it exhibits a lamellar bone structure at 16 weeks of age.

Spectral images obtained from each section were analyzed using ISYS Chemical Imaging Software (Spectral Dimensions, Olney, MD, USA). After spectral subtraction of embedding medium (PMMA), the following parameters were calculated from the corrected spectra: mineral-to-matrix area ratio ([916-1180 cm^{-1}]/[1588-1712 cm^{-1}]) [31], carbonate-to-matrix area ratio ([840-890 cm^{-1}]/[1588-1712 cm^{-1}]) [32,33], carbonate-to-mineral area ratio [(840-890 cm^{-1}]/[916-1180 cm^{-1}]) [32,33], collagen cross-linking ratio (XLR) (1660/1690 cm^{-1}) [34], crystallinity (1030/1020 cm^{-1}) [35,36], and acid phosphate (1106/960 cm^{-1}) [36, 37] (Fig. 1). Each of these parameters except XLR has been validated by independent methods [38,39]. XLR has been associated with the ratio of reducible/nonreducible cross-links [34] and, for the purpose of this report, will be referred to as “collagen maturity.” Mean values for each animal (mean of two to three sections) were then averaged to give a strain-averaged value for each measured trait. For each of these IR spectral parameters, variation in pixel distribution was quantified by fitting a Gaussian curve to the data and calculating the width of the curve at half-maximum. Samples that were more homogeneous in their pixel distribution for a given trait therefore had a smaller curve width at half-maximum. Carbonate bands were curve-fit using public domain software (Moffatt, Canadian Research Council) to determine the percentage of hydroxyl-substituted type A (871-873 cm^{-1}), phosphate-substituted type B (878-879 cm^{-1}), and labile carbonate (865-867 cm^{-1}) within each sample.

Mechanical Properties

Right femora from a second group of comparably aged but distinct animals—A/J (n = 10), B6 (n = 14), and C3H (n = 7)—were cleaned and the epiphyses embedded in brass pots with Scotch-Weld acrylic adhesive DP-810 (3 M, St. Paul, MN, USA). Potted bone samples were machined to yield a gauge region comprised of only the anterior portion of the femoral diaphysis. The anterior region was chosen for analysis because at 16 weeks of age this bone tissue has a largely lamellar, cortical structure. Anterior regions for each test specimen were machined on their medial and lateral sides to create gauge lengths of 3 mm and widths of 280 μm under constant

PBS irrigation using an automated CNC milling machine (model MDX-20; Roland DGA, Irvine, CA, USA) (Fig. 2). To minimize microstructural defects from machining, the periosteal and endosteal surfaces of each anterior specimen were not machined but quantitative dimensional measurements were obtained using image analysis (see below). Although studies of bending loads are relevant to fracture, bending induces a cross-hatch fracture pattern in the compressive region which combines the effects of tissue ultrastructure and lamellar organization [40]. In tensile loading, failure appears to initiate at the ultrastructural level. Consequently, a tensile loading regimen was chosen to better relate tissue-level mechanical properties to ultrastructural variation in mineral and matrix and not the higher-order lamellar structure of bone. Tissue-level mechanical properties were obtained by loading milled samples in tension at 10 μm/sec using a servo-hydraulic materials testing system (model 8872; Instron, Canton, MA, USA). Tensile deformations were accurately measured using a noncontacting imaging system consisting of a high-resolution digital video camera (RH1100; Duncan Tech, Auburn, CA, USA) and a video zoom microscope lens (Edmund Industrial Optics, Barrington, NJ, USA) with a resolution of 2.3 μm [41]. Bending loads were minimized through precise alignment of all test fixtures using a micrometer stage. Further, minimum bending loads were confirmed based on minimal side-to-side displacement of the sample after failing. Images were taken every 0.1 seconds (10 times per second) during loading. During potting and testing, all samples were kept moist using PBS supplemented with calcium chloride [42].

For each digital image, sample strain values were calculated using digital-image correlation (IMAQ Vision Builder 6.0; National Instruments, Austin, TX, USA) by tracking the movement (linear distance in two dimensions) of clusters of 16-μm silicon carbide particles (McMaster-Carr, Elmhurst, IL, USA) (Fig. 2) located just outside the proximal and distal thirds of the gauge region so as to minimize irregularities from local deformations. Although our camera resolution was 2.3 μm, digital-image correlation affords a higher (subpixel) resolution by tracking the change in distance of the centroids of the two silicon carbide clusters. Since only the medial and lateral sides of the anterior quadrants were milled, true stress values were calculated by dividing force data by the actual cross-sectional area of samples after failure. First, the fractured samples were stained with basic fuchsin, embedded in Caroplastic (Carolina Biological Supply, Burlington, NC, USA) and sectioned transversely (200 μm) using a low-speed diamond-coated wafering saw (Buehler, Lake Bluff, IL, USA). Next, sections were fixed to acrylic slides, polished to a 1 μm finish, and imaged with a digital Exwave HAD 3CCD camera (Sony, New York, NY, USA) and light microscope (Axioplan2; Carl Zeiss IMT, Minneapolis, MN, USA) with a pixel resolution of 0.286 μm. Cross-sectional areas of three to six sections/sample were measured using IMAQ Vision Builder 6.0 (National Instruments) and the values averaged. Sample dimensions did not vary significantly before and after testing (data not shown). Stress/strain curves of approximately 100 data points were created to determine strength, post-yield strain, work-to-failure, and Young's modulus (modulus) (Fig. 3). Modulus values were calculated from the initial, linear portion of the curve before yield; yield was defined as a 0.2% offset. Although samples were loaded at constant displacement, the testing apparatus is not a uniform structure and differences in the component material properties can affect the actual strain rate of the sample gauge region. Under this experimental setup, each sample will deform at slightly different rates depending on the compliance of these additional interfaces and materials. We accounted for strain rate variation by regressing each modulus value to the average strain rate of all A/J, B6, and C3H animals, thereby further improving our precision and enabling us to better differentiate tissue-level properties among the inbred strains. The overall accuracy of our mechanical testing and imaging methods was verified using milled aluminum samples of known mechanical properties; our calculated modulus for milled aluminum samples (n = 6) was 74.2 ± 6.8 GPa compared to the published value of ~70 GPa.

Morphological Traits

To determine how tissue-level variation in spectral parameters and mechanical properties relate to whole-bone morphology, whole-bone morphological traits were measured. From the cohort of mice used for FTIRI analyses, contralateral (left) femora were taken for analysis of morphology. In addition, femora used for tissue-level mechanical testing were analyzed for morphological traits. Diaphyseal, transverse morphology was measured using the eXplore Locus SP Pre-Clinical Specimen MicroComputed Tomography System (GE Healthcare, London, Canada). Three-dimensional images of whole femora were obtained at an 8.7 μm voxel size, and analyses were performed on a 2.5-mm-tall region beginning distal to the third trochanter. Total area (Tt.Ar), cortical Area (Ct.Ar), marrow area (Ma.Ar), and polar moment of inertia (J_o) were calculated as previously described [29]. Cortical thickness (Ct.Th) was calculated as 2x(Ct.Ar)/(periosteal perimeter + endosteal perimeter). Femoral length (Le) was measured from the most proximal tip of the femoral head to the bottom of the distal epiphysis.

Statistical Analyses

Mean values for FTIRI spectral parameters and mechanical properties were calculated for each strain, and significant differences were assessed using ANOVA and Bonferroni post-hoc tests with a significance threshold of $P < 0.05$ (Statistica 6.0; Statsoft, Tulsa, OK, USA). To correlate FTIRI parameters and tissue-level mechanical properties with their associated whole-bone morphological traits, Pearson correlations were calculated for trait comparisons using the raw data from individual strains and the raw data pooled across strains. For each correlation analysis, the threshold for $P < 0.05$ significance was chosen using permutation tests in order to correct for multiple comparisons and determine the maximum coefficient arising from a random distribution of trait values across individuals [43,44]. Due to the known broadening of the acid phosphate subbands with decreasing mineral content and crystallinity, statistical correlations using our acid phosphate data were not performed [37,45]. For all other traits, significant Pearson correlations were noted and then analyzed, where appropriate, using linear regressions for individual strain data and for data pooled across all three strains (GraphPad Software, San Diego, CA, USA).

Results

Compositional Traits

Results from FTIRI analyses revealed significant variation between at least two strains for all spectral parameters except crystallinity (Table 1, Fig. 4). Significant differences were found in the comparison of A/J and C3H mean trait values. C3H femora demonstrated a mineral-to-amide I area ratio (8.0 ± 0.4) that was intermediate of A/J (8.4 ± 0.7) and B6 (7.5 ± 0.4). C3H carbonate-to-amide I and carbonate-to-mineral area ratios were both significantly lower (18% and 11%, respectively) than values for A/J. Curve-fitting of carbonate bands revealed no significant differences in the amount of type A, type B, and labile carbonate substituted in the three strains (data not shown). Mean acid phosphate values for C3H were 23% lower than those for A/J. Mean values for XLR revealed significant differences among all three stains, with C3H having the greatest collagen maturity. Femora from A/J and B6 had collagen XLRs that were 11% smaller and statistically indistinguishable from each other. To determine if the pixel distribution for each trait varied among strains, a Gaussian distribution was fit to the pixel histograms for each spectral parameter. Results revealed that only XLR differed significantly in its pixel distribution, as evidenced by a 62% increase in curve width at half-maximum for the C3H strain (Fig. 5).

Mechanical Properties

Significant differences in mechanical properties were found between A/J and B6 femora (Table 2). A/J femora had a significantly larger (21%) modulus (34.9 ± 4.4 GPa) than B6 femora (27.4 ± 4.1 GPa). However, B6 femora performed 47% more work-to-failure (1.50 ± 0.71 MPa) than A/J femora (0.8 ± 0.49 MPa) and demonstrated nearly 60% more total strain, indicating that although A/J femora are stiffer at the tissue level, they are also more brittle. The mean modulus and work-to-failure for C3H femora were both found to be intermediate of A/J and B6. Although the post-yield strain of A/J femora was one-third less than that of B6 and C3H femora, no significant differences in post-yield strain were found among the three strains. In addition, strength was not significantly different among the three strains.

Correlation Analyses

Correlation analyses were performed among whole-bone morphological traits and their corresponding compositional traits or tissue-level mechanical properties. For comparisons within strain, there were no significant composition-morphology relationships. However, when data were pooled across strains, significant differences were found, indicating intraspecies variation in trait relationships. Significant correlations were found among spectral traits ($R \geq 0.68$, $P < 0.05$) but not between spectral traits and whole-bone morphological traits. A significant correlation ($R \geq 0.86$) between carbonate-to-amide I mean ratio and carbonate-to-mineral mean ratio was observed. In addition, both carbonate-to-amide I and carbonate-to-mineral mean ratios were negatively correlated with cross-link maturity ($R \geq -0.70$ and -0.69, respectively). Linear regressions were applied to trait relationships with significant Pearson correlations (Fig. 6). In all cases the slopes of lines fit to the individual strain data were statistically indistinguishable ($P < 0.05$) and only the regression lines for data pooled across strains are shown, confirming that trait variation within strains is minimal.

After pooling data across strains, significant correlations were found among tissue-level mechanical properties and whole-bone morphological traits ($R \geq 0.56$, $P < 0.05$) but only for modulus. A significant negative correlation was found between modulus and both Tt.Ar and Ma.Ar ($R \geq -0.58$ and -0.70, respectively). Given that morphological traits and modulus values cluster when regressed against each other, linear regressions were not performed for these significant correlations. However, a clear trend of increasing modulus with increasing slenderness (decreasing Tt.Ar/Le) was observed (Fig. 7).

Discussion

Compositional Traits

Comparisons across species have demonstrated that variation in bone matrix composition is not random but part of a biological paradigm to establish function [13,16,17]. This investigation focused on variation within species and found significant intraspecies variation in femoral tissue-level composition, maturity, and mechanical properties, suggesting that genetic variation defines mechanically relevant bone traits at the tissue level. Femoral ash content [2, 28] and BMD [46] are known to vary among inbred mice, and we confirmed these findings at the tissue level with our measurements of mineral-to-amide mean area ratios. These results are consistent with prior studies showing that mineral-to-amide I values are correlated with ash content in synthetic mixtures of mineral and collagen and in bones from dogs and humans [31,47]. The observed mineral-to-amide I and ash content variations indicate that A/J, C3H, and B6 mice regulate mineralization at the tissue level by packing different amounts of mineral into the collagen network. This finding supports prior work correlating increases in whole-bone mineral content with increased stiffness at the expense of decreased post-yield strain (increased brittleness) in A/J femora [27].

In addition to differences in the amount of mineral, we observed that the mineral structure at 16 weeks of age is different among A/J, C3H, and B6 femora. Although the type of carbonate substitution did not differ significantly among strains, C3H femora had a smaller total amount of carbonate relative to mineral and amide I compared to A/J and B6 femora. This indicates that the mineralization process in C3H femora limits the number of OH^- and PO_4^{3-} groups replaced by carbonate. Similarly, acid phosphate was less prevalent in C3H femora, indicating it has a more stoichiometric apatite than A/J and B6. Acid phosphate is associated with immature, more labile mineral crystals [37] and the presence of increased carbonate substitutions in hydroxyapatite has been linked to increased apatite dissolution [48] and osteoclastic resorption [49]. In C3H femora, deposition of mineral with reduced levels of acid phosphate and carbonate may represent a mechanism for promoting increased bone formation [2,50,51] and decreased bone resorption [2,52] that is additional to known regulatory pathways such as receptor activator of nuclear factor κ (RANK)-dependent regulation of cellular activity. This variation may help explain the increased Ct.Th of C3H relative to A/J and B6 mice.

Despite differences in mineral composition, which might imply that the crystallinity of C3H femora is also greater, there were no significant differences in crystallinity as assessed from the FTIRI parameters among the three mouse strains. Although the measured crystallinity (defined from FTIR 1030/1020 ratio as average crystal size/perfection as correlated with XRD analyses [31]) tended to increase with increased mineral-to-matrix ratio [53], significant differences were not detected, reflecting the lack of sensitivity of the crystallinity parameter as determined by a peak height ratio of 1030/1020 cm^{-1} subbands [54]. There are other cases where mineral content increases and crystallinity does not. For example, in younger osteonectin-null mice, an increase in mineral-to-matrix ratio accompanied a decrease in crystallinity [54]; and in ovariectomized mice, there was no change in crystallinity with increasing mineral-to-matrix ratio [55]. Also, in biglycan knockout mice, ash content and mineral-to-matrix ratios decreased but crystallinity, as determined by X-ray diffraction, did not change [56]. Increased crystallinity has been associated with bone brittleness [57], and while C3H femora had an increase in mineral content and modulus relative to B6, there was no increase in tissue-level brittleness or crystallinity. Thus, the biological mechanism responsible for an increase in C3H femoral mineral content and modulus appears to be fortuitously associated with no increase in tissue-level brittleness. Further, if a decrease in carbonate and acid phosphate content of C3H femora did serve to protect against bone resorption and promote endosteal in-filling, then mineral of increased crystallinity would also be expected since it is less resistant to dissolution. However, C3H femora had statistically comparable crystallinity values for A/J and B6, and this may indicate that genetic regulation of other variables (carbonate, acid phosphate, collagen cross-linking) may be able to compensate to maintain functionality (i.e., larger modulus with no increase in brittleness).

Significant collagen matrix differences were observed as evidenced by the FTIRI of C3H femora having a greater XLR; increases in XLR have been associated with increases in matrix maturity [34,58,59]. This confirms prior work reporting that C3H humeri and tibiae had more mature, pyridinoline cross-links than B6 [60]. Interestingly, the distribution of these mature cross-links in C3H femora varied such that there were regions of cross-link maturity similar to A/J and B6 as well as regions with much greater cross-link maturity (Fig. 4). There was no consistent spatial variation for these regions of high and low cross-link maturity, indicating that C3H femora may exhibit significant spatial variation in matrix maturity.

Previous studies have reported tissue-level variation in the compositional parameters examined here. For example, variable tissue-level mineral content [53,54,61,62], carbonate content [53,63], and collagen cross-link maturity [34,64] have been documented. Although these studies are informative, they are a function of either a disease state or variable animal/tissue age. The present study is one of the first investigations demonstrating that different adult tissue-

level bone mineral composition and matrix maturity phenotypes can simultaneously arise from natural genetic variation within species. The observed phenotypic differences suggest that intraspecies genetic variation gives rise to differential cellular control over mineral and matrix maturity during growth and development. Consequently, multiple bone quality phenotypes can be formed and are able to exist within variable, but mechanically functional, whole-bone structures [28,29].

Mechanical Properties

Accompanying variation in tissue-level composition, A/J, C3H, and B6 mice exhibited significant differences in tissue-level mechanical properties. Prior to this investigation, whole-bone morphological traits and ash content have been reported for these three strains and variation in these traits explained 66-88% of the variability in whole-bone mechanical properties [28]. It was therefore expected, but unconfirmed, that variation at the tissue level would also influence whole-bone functionality. Our results demonstrate that variation at the tissue level is significant and is in agreement with whole-bone mechanical data. Given that A/J femora have greater mineral content than C3H and B6 and mineral content is highly correlated with stiffness, a greater modulus value for A/J femora was expected. However, at the whole-bone level A/J stiffness no longer exceeds B6, and this is because geometry must be taken into account: A/J femora are more slender. Similarly, the intermediate mineral content and modulus for C3H translate to a whole-bone stiffness that is much larger than that of both A/J and B6 by virtue of C3H's large Ct.Ar.

Variation in tissue-level strength and post-yield strain mirrored whole-bone values for the three strains [28], though no statistical differences were found. It should be noted that the variability of post-yield strain does not indicate a lack of experimental precision. Since post-yield strain is a parameter that describes the failure process, measurements are typically very complicated and heterogeneous. Prior studies measuring post-yield strain at the whole-bone level also reported tremendous variability [28,29]. One of the reasons we machined only two sides of each bone was to minimize machining defects that might enhance variability in post-yield strain. That our tissue-level post-yield strain and total strain data support variation in mineral content is testimony to the accuracy of the approach (we thought the variability might obscure all tissue-level trends among mice, but the trends were still observable). We expect that if technology advances to provide more accurate values for failure properties of such small specimens, the mean values obtained will still be in line with those found in our investigation.

Differences in tissue-level work-to-failure also mirrored whole-bone values, and significant differences were observed between A/J and B6 femora. As expected, A/J femora exhibited a brittle (nonductile) failure behavior with minimal post-yield strain and as a result performed the least amount of work-to-failure. In addition to the contribution from increased mineral, increased acid phosphate levels and decreased collagen cross-link maturity may contribute to the brittleness of A/J femora. Support for this theory is found in a study where the occurrence of vertebral microdamage was associated with local increases in acid phosphate and decreases in collagen cross-link maturity [65].

It should be noted that a number of investigations have reported tissue-level mechanical properties for bone tissues and these values can vary by an order of magnitude. Recent studies using nanoindentation on adult mouse [66-68], rat [5], and human [69] femoral cortices gave modulus values of 15-33 GPa. On the other hand, in studies that determined modulus through back-calculations [59,70,71] or through mechanical testing with "grip-to-grip" calculations, where sample strain is assumed to be identical to the strain of the grips holding the sample [72], modulus values were significantly lower (1-6 GPa) compared to our current results (27-34 GPa). We confirmed this experimental variation by calculating our modulus values using grip-to-grip displacements and by back-calculating from whole-bone mechanical properties. Using

these approaches, we obtained modulus values of 5-6 and 2-5 GPa, respectively (data not shown). In addition, differences in mean values among strains are no longer apparent using these approaches. Thus, nanoindentation and tissue-level mechanical testing with true strain values appear to give more accurate values for tissue-level mechanical properties. In support of this, we constructed an updated plot of tissue-level stiffness (modulus) versus ash content using our mouse data and a variety of published bone data ranging from deer to whale (Fig. 8). There is a strong correlation between the two variables as originally noted by Currey [17]; and our measured values for A/J, C3H,and B6 femora fall near those for human and bovine femora measured using similar experimental methods.

Correlation Analyses

Significant correlations were found among FTIRI spectral parameters. As expected, carbonate-to-mineral mean ratios were positively correlated with carbonate-to-amide I mean ratios, confirming that our carbonate changes are independent of changes of mineral or amide I. Carbonate-to-mineral and carbonate-to-amide I mean ratios were each negatively correlated with collagen maturity. Although the relationship between collagen maturity and bone formation/resorption is unclear, the association of lower concentrations of carbonate with increased collagen cross-link maturity suggests that mineral composition and matrix maturity may covary during growth to permit increased bone formation and decreased bone resorption.

Mean modulus values were found to vary among A/J, B6, and C3H such that mice with more slender bones (small Tt.Ar relative to Le, A/J) tend to contain stiffer material, whereas mice with larger bones (large Tt.Ar relative to Le, B6) contain less stiff material (Fig. 7). This trend is in agreement with prior work on human samples showing that smaller tibiae had increased moduli and were more brittle than larger tibiae [73]. C3H femora are intermediate to A/J and B6 in both modulus and slenderness. However, given that C3H femora have increased Ct.Ar relative to both A/J and B6, the need for increased tissue-level mechanical properties (modulus) seems redundant. Despite this difference, we know that C3H femora still covary mineral deposition and whole-bone morphology during growth and in a manner consistent with A/J and B6 [2]. Future studies are needed to determine if the increased Ct.Ar is truly redundant or if it plays a specialized mechanical or physiological role.

Conclusions

This investigation has demonstrated that, within species, genetic variation can give rise to phenotypic variation in the tissue quality of bone (mineral composition, matrix maturity) and that this variation is matched to whole-bone morphology, thereby creating bones that are functional for normal loads. Variation in mineral and matrix traits can be found in a variety of animal models, and given that associations between bone quality, morphology, and mechanical properties have been reported in many species, this likely represents a global biological paradigm for the regulation of trait covariation. The cellular processes directing variation in bone quality and morphological phenotypes are likely shared by a number of species and close correlation between mouse and human confirm that inbred mice are a good model for studying skeletal functionality and fracture susceptibility. Future studies examining genetic disruption of bone quality and morphology, as well as studies during growth, will shed light on the cellular and molecular mechanisms that permit the creation of functional and nonfunctional skeletal phenotypes.

Acknowledgements

The authors thank Damien Laudier for assistance with plastic embedding and the National Institutes of Health (NIH) for funding support (AR44927, AR046121). FTIR images were obtained using the NIH-sponsored Core Center (AR046121) at the Hospital for Special Surgery.

References

1. Reeves GM, McCreadie BR, Shu C, Galecki AT, Burke DT, Miller RA, Goldstein SA. Quantitative trait loci modulate vertebral morphology and mechanical properties in a population of 18-month-old genetically heterogeneous mice. Bone 2006;40:433–443. [PubMed: 17049325]
2. Price C, Herman BC, Lufkin T, Goldman HM, Jepsen KJ. Genetic variation in bone growth patterns defines adult mouse bone fragility. J Bone Miner Res 2005;20:1983–1991. [PubMed: 16234972]
3. Martens M, Van Audekercke R, De Meester P, Mulier JC. The geometrical properties of human femur and tibia and their importance for the mechanical behaviour of these bone structures. Arch Orthop Trauma Surg 1981;98:113–120. [PubMed: 7294986]
4. Nyman JS, Roy A, Tyler JH, Acuna RL, Gayle HJ, Wang X. Age-related factors affecting the postyield energy dissipation of human cortical bone. J Orthop Res 2007;25:646–655. [PubMed: 17266142]
5. Busa B, Miller LM, Rubin CT, Qin YX, Judex S. Rapid establishment of chemical and mechanical properties during lamellar bone formation. Calcif Tissue Int 2005;77:386–394. [PubMed: 16362460]
6. Bouxsein ML, Uchiyama T, Rosen CJ, Shultz KL, Donahue LR, Turner CH, Sen S, Churchill GA, Muller R, Beamer WG. Mapping quantitative trait loci for vertebral trabecular bone volume fraction and microarchitecture in mice. J Bone Miner Res 2004;19:587–599. [PubMed: 15005846]
7. Turner CH. Bone strength: current concepts. Ann N Y Acad Sci 2006;1068:429–446. [PubMed: 16831941]
8. Blake GM, Fogelman I. The role of DXA bone density scans in the diagnosis and treatment of osteoporosis. Postgrad Med J 2007;83:509–517. [PubMed: 17675543]
9. Turner CH. Biomechanics of bone: determinants of skeletal fragility and bone quality. Osteoporos Int 2002;13:97–104. [PubMed: 11905527]
10. Rivadeneira F, Zillikens MC, De Laet CE, Hofman A, Uitter-linden AG, Beck TJ, Pols HA. Femoral neck BMD is a strong predictor of hip fracture susceptibility in elderly men and women because it detects cortical bone instability: the Rotterdam Study. J Bone Miner Res 2007;22:1781–1790. [PubMed: 17638578]
11. Wergedal JE, Sheng MH, Ackert-Bicknell CL, Beamer WG, Baylink DJ. Genetic variation in femur extrinsic strength in 29 different inbred strains of mice is dependent on variations in femur cross-sectional geometry and bone density. Bone 2005;36:111–122. [PubMed: 15664009]
12. Burr DB, Forwood MR, Fyhrie DP, Martin RB, Schaffler MB, Turner CH. Bone microdamage and skeletal fragility in osteoporotic and stress fractures. J Bone Miner Res 1997;12:6–15. [PubMed: 9240720]
13. Currey JD. The relationship between the stiffness and the mineral content of bone. J Biomech 1969;2:477–480. [PubMed: 16335147]
14. Currey JD. Effects of differences in mineralization on the mechanical properties of bone. Philos Trans R Soc Lond B Biol Sci 1984;304:509–518. [PubMed: 6142490]
15. Currey JD. Tensile yield in compact bone is determined by strain, postyield behaviour by mineral content. J Biomech 2004;37:549–556. [PubMed: 14996567]
16. Zioupos P, Currey JD, Casinos A. Exploring the effects of hypermineralisation in bone tissue by using an extreme biological example. Connect Tissue Res 2000;41:229–248. [PubMed: 11264871]
17. Currey JD. The mechanical consequences of variation in the mineral content of bone. J Biomech 1969;2:1–11. [PubMed: 16335107]
18. Currey JD. Mechanical properties of bone tissues with greatly differing functions. J Biomech 1979;12:313–319. [PubMed: 468855]
19. Martin RB, Ishida J. The relative effects of collagen fiber orientation, porosity, density, and mineralization on bone strength. J Biomech 1989;22:419–426. [PubMed: 2777816]
20. Martin RB, Boardman DL. The effects of collagen fiber orientation, porosity, density, and mineralization on bovine cortical bone bending properties. J Biomech 1993;26:1047–1054. [PubMed: 8408087]
21. Oxlund H, Barckman M, Ortoft G, Andreassen TT. Reduced concentrations of collagen cross-links are associated with reduced strength of bone. Bone 1995;17:365S–371S. [PubMed: 8579939]
22. Oxlund H, Mosekilde L, Ortoft G. Reduced concentration of collagen reducible cross links in human trabecular bone with respect to age and osteoporosis. Bone 1996;19:479–484. [PubMed: 8922646]

23. Papadimitriou HM, Swartz SM, Kunz TH. Ontogenic and anatomic variation in mineralization of the wing skeleton of the Mexican free-tailed bat, *Tadarida brasiliensis*. J Zool (Lond) 1996;240:411–426.
24. Marshall D, Johnell O, Wedel H. Meta-analysis of how well measures of bone mineral density predict occurrence of osteoporotic fractures. BMJ 1996;312:1254–1259. [PubMed: 8634613]
25. Lafleur J, McAdam-Marx C, Kirkness C, Brixner DI. Clinical risk factors for fracture in postmenopausal osteoporotic women: a review of the recent literature. Ann Pharmacother 2008;42:375–386. [PubMed: 18230704]
26. McCreadie BR, Goldstein SA. Biomechanics of fracture: is bone mineral density sufficient to assess risk? J Bone Miner Res 2000;15:2305–2308. [PubMed: 11127195]
27. Jepsen KJ, Pennington DE, Lee YL, Warman M, Nadeau J. Bone brittleness varies with genetic background in A/J and C57BL/6 J inbred mice. J Bone Miner Res 2001;16:1854–1862. [PubMed: 11585350]
28. Jepsen KJ, Akkus OJ, Majeska RJ, Nadeau JH. Hierarchical relationship between bone traits and mechanical properties in inbred mice. Mamm Genome 2003;14:97–104. [PubMed: 12584605]
29. Jepsen KJ, Hu B, Tommasini SM, Courtland HW, Price C, Terranova CJ, Nadeau JH. Genetic randomization reveals functional relationships among morphologic and tissue-quality traits that contribute to bone strength and fragility. Mamm Genome 2007;18:492–507. [PubMed: 17557179]
30. Beamer WG, Donahue LR, Rosen CJ, Baylink DJ. Genetic variability in adult bone density among inbred strains of mice. Bone 1996;18:397–403. [PubMed: 8739896]
31. Faibish D, Gomes A, Boivin G, Binderman I, Boskey A. Infrared imaging of calcified tissue in bone biopsies from adults with osteomalacia. Bone 2005;36:6–12. [PubMed: 15663997]
32. Mayer I, Schneider S, Sydney-Zax M, Deutsch D. Thermal decomposition of developing enamel. Calcif Tissue Int 1990;46:254–257. [PubMed: 2108795]
33. Rey C, Collins B, Goehl T, Dickson IR, Glimcher MJ. The carbonate environment in bone mineral: a resolution-enhanced Fourier transform infrared spectroscopy study. Calcif Tissue Int 1989;45:157–164. [PubMed: 2505907]
34. Paschalis EP, Verdelis K, Doty SB, Boskey AL, Mendelsohn R, Yamauchi M. Spectroscopic characterization of collagen cross-links in bone. J Bone Miner Res 2001;16:1821–1828. [PubMed: 11585346]
35. Pleshko N, Boskey A, Mendelsohn R. Novel infrared spectroscopic method for the determination of crystallinity of hydroxyapatite minerals. Biophys J 1991;60:786–793. [PubMed: 1660314]
36. Gadaleta SJ, Paschalis EP, Betts F, Mendelsohn R, Boskey AL. Fourier transform infrared spectroscopy of the solution-mediated conversion of amorphous calcium phosphate to hydroxyapatite: new correlations between X-ray diffraction and infrared data. Calcif Tissue Int 1996;58:9–16. [PubMed: 8825233]
37. Rey C, Shimizu M, Collins B, Glimcher MJ. Resolution-enhanced Fourier transform infrared spectroscopy study of the environment of phosphate ion in the early deposits of a solid phase of calcium phosphate in bone and enamel and their evolution with age: 2. Investigations in the nu3PO4 domain. Calcif Tissue Int 1991;49:383–388. [PubMed: 1818762]
38. Boskey A, Mendelsohn R. Infrared analysis of bone in health and disease. J Biomed Opt 2005;10:031102. [PubMed: 16229627]
39. Boskey A, Mendelsohn R. Infrared spectroscopic characterization of mineralized tissues. Vibrat Spectrosc 2005;38:107–114.
40. Jepsen KJ, Goldstein SA, Kuhn JL, Schaffler MB, Bonadio J. Type-I collagen mutation compromises the postyield behavior of Mov13 long bone. J Orthop Res 1996;14:493–499. [PubMed: 8676263]
41. Tommasini SM, Morgan TG, van der Meulen M, Jepsen KJ. Genetic variation in structure-function relationships for the inbred mouse lumbar vertebral body. J Bone Miner Res 2005;20:817–827. [PubMed: 15824855]
42. Gustafson M, Martin R, Gibson V, Storms D, Stover S, Gibeling J, Griffin L. Calcium buffering is required to maintain bone stiffness in saline solution. J Biomech 1996;29:1191–1194. [PubMed: 8872276]
43. Churchill GA, Doerge RW. Empirical threshold values for quantitative trait mapping. Genetics 1994;138:963–971. [PubMed: 7851788]

44. Nadeau JH, Burrage LC, Restivo J, Pao YH, Churchill G, Hoit BD. Pleiotropy, homeostasis, and functional networks based on assays of cardiovascular traits in genetically randomized populations. Genome Res 2003;13:2082–2091. [PubMed: 12952877]
45. Miller LM, Vairavamurthy V, Chance MR, Mendelsohn R, Paschalis EP, Betts F, Boskey AL. In situ analysis of mineral content and crystallinity in bone using infrared micro-spectroscopy of the $nu_4PO_4^{3-}$ vibration. Biochim Biophys Acta 2001;1527:11–19. [PubMed: 11420138]
46. Ng AH, Wang SX, Turner CH, Beamer WG, Grynpas MD. Bone quality and bone strength in BXH recombinant inbred mice. Calcif Tissue Int 2007;81:215–223. [PubMed: 17638038]
47. Pienkowski D, Doers TM, Monier-Faugere MC, Geng Z, Camacho NP, Boskey AL, Malluche HH. Calcitonin alters bone quality in beagle dogs. J Bone Miner Res 1997;12:1936–1943. [PubMed: 9383698]
48. LeGeros RZ, Kijkowska R, Bautista C, LeGeros JP. Synergistic effects of magnesium and carbonate on properties of biological and synthetic apatites. Connect Tissue Res 1995;33:203–209. [PubMed: 7554956]
49. Doi Y, Iwanaga H, Shibutani T, Moriwaki Y, Iwayama Y. Osteoclastic responses to various calcium phosphates in cell cultures. J Biomed Mater Res 1999;47:424–433. [PubMed: 10487896]
50. Sheng MH, Baylink DJ, Beamer WG, Donahue LR, Rosen CJ, Lau KH, Wergedal JE. Histomorphometric studies show that bone formation and bone mineral apposition rates are greater in C3H/HeJ (high-density) than C57BL/6 J (low-density) mice during growth. Bone 1999;25:421–429. [PubMed: 10511108]
51. Richman C, Kutilek S, Miyakoshi N, Srivastava AK, Beamer WG, Donahue LR, Rosen CJ, Wergedal JE, Baylink DJ, Mohan S. Postnatal and pubertal skeletal changes contribute pre-dominantly to the differences in peak bone density between C3H/HeJ and C57BL/6 J mice. J Bone Miner Res 2001;16:386–397. [PubMed: 11204439]
52. Linkhart TA, Linkhart SG, Kodama Y, Farley JR, Dimai HP, Wright KR, Wergedal JE, Sheng M, Beamer WG, Donahue LR, Rosen CJ, Baylink DJ. Osteoclast formation in bone marrow cultures from two inbred strains of mice with different bone densities. J Bone Miner Res 1999;14:39–46. [PubMed: 9893064]
53. Paschalis EP, DiCarlo E, Betts F, Sherman P, Mendelsohn R, Boskey AL. FTIR microspectroscopic analysis of human osteonal bone. Calcif Tissue Int 1996;59:480–487. [PubMed: 8939775]
54. Boskey AL, Moore DJ, Amling M, Canalis E, Delany AM. Infrared analysis of the mineral and matrix in bones of osteonectin-null mice and their wildtype controls. J Bone Miner Res 2003;18:1005–1011. [PubMed: 12817752]
55. Boskey AL, Gadaleta S, Gundberg C, Doty SB, Ducy P, Karsenty G. Fourier transform infrared microspectroscopic analysis of bones of osteocalcin-deficient mice provides insight into the function of osteocalcin. Bone 1998;23:187–196. [PubMed: 9737340]
56. Xu T, Bianco P, Fisher LW, Longenecker G, Smith E, Goldstein S, Bonadio J, Boskey A, Heegaard AM, Sommer B, Satomura K, Dominguez P, Zhao C, Kulkarni AB, Robey PG, Young MF. Targeted disruption of the biglycan gene leads to an osteoporosis-like phenotype in mice. Nat Genet 1998;20:78–82. [PubMed: 9731537]
57. Freeman JJ, Wopenka B, Silva MJ, Pasteris JD. Raman spectroscopic detection of changes in bioapatite in mouse femora as a function of age and in vitro fluoride treatment. Calcif Tissue Int 2001;68:156–162. [PubMed: 11351499]
58. Paschalis EP, Shane E, Lyritis G, Skarantavos G, Mendelsohn R, Boskey AL. Bone fragility and collagen cross-links. J Bone Miner Res 2004;19:2000–2004. [PubMed: 15537443]
59. Blank RD, Baldini TH, Kaufman M, Bailey S, Gupta R, Yershov Y, Boskey AL, Coppersmith SN, Demant P, Paschalis EP. Spectroscopically determined collagen Pyr/deH-DHLNL cross-link ratio and crystallinity indices differ markedly in recombinant congenic mice with divergent calculated bone tissue strength. Connect Tissue Res 2003;44:134–142. [PubMed: 14504033]
60. Amblard D, Lafage-Proust MH, Chamson A, Rattner A, Collet P, Alexandre C, Vico L. Lower bone cellular activities in male and female mature C3H/HeJ mice are associated with higher bone mass and different pyridinium crosslink profiles compared to C57BL/6J mice. J Bone Miner Metab 2003;21:377–387. [PubMed: 14586794]

61. Boskey AL, Marks SC Jr. Mineral and matrix alterations in the bones of incisors-absent (ia/ia) osteopetrotic rats. Calcif Tissue Int 1985;37:287–292. [PubMed: 3926278]
62. Shapses SA, Cifuentes M, Spevak L, Chowdhury H, Brittingham J, Boskey AL, Denhardt DT. Osteopontin facilitates bone resorption, decreasing bone mineral crystallinity and content during calcium deficiency. Calcif Tissue Int 2003;73:86–92. [PubMed: 14506959]
63. Camacho NP, Rimnac CM, Meyer RA Jr, Doty S, Boskey AL. Effect of abnormal mineralization on the mechanical behavior of X-linked hypophosphatemic mice femora. Bone 1995;17:271–278. [PubMed: 8541141]
64. Paschalis EP, Burr DB, Mendelsohn R, Hock JM, Boskey AL. Bone mineral and collagen quality in humeri of ovariectomized cynomolgus monkeys given rhPTH(1-34) for 18 months. J Bone Miner Res 2003;18:769–775. [PubMed: 12674338]
65. Ruppel ME, Burr DB, Miller LM. Chemical makeup of microdamaged bone differs from undamaged bone. Bone 2006;39:318–324. [PubMed: 16584933]
66. Silva MJ, Brodt MD, Fan Z, Rho JY. Nanoindentation and whole-bone bending estimates of material properties in bones from the senescence accelerated mouse SAMP6. J Biomech 2004;37:1639–1646. [PubMed: 15388305]
67. Akhter MP, Fan Z, Rho JY. Bone intrinsic material properties in three inbred mouse strains. Calcif Tissue Int 2004;75:416–420. [PubMed: 15592798]
68. Miller LM, Little W, Schirmer A, Sheik F, Busa B, Judex S. Accretion of bone quantity and quality in the developing mouse skeleton. J Bone Miner Res 2007;22:1037–1045. [PubMed: 17402847]
69. Wang X, Sudhaker Rao D, Ajdelsztajn L, Ciarelli TE, Lavernia EJ, Fyhrie DP. Human iliac crest cancellous bone elastic modulus and hardness differ with bone formation rate per bone surface but not by existence of prevalent vertebral fracture. J Biomed Mater Res B Appl Biomater 2007;85:68–77. [PubMed: 17696151]
70. Wang XD, Masilamani NS, Mabrey JD, Alder ME, Agrawal CM. Changes in the fracture toughness of bone may not be reflected in its mineral density, porosity, and tensile properties. Bone 1998;23:67–72. [PubMed: 9662132]
71. Yershov Y, Baldini TH, Villagomez S, Young T, Martin ML, Bockman RS, Peterson MG, Blank RD. Bone strength and related traits in HcB/Dem recombinant congenic mice. J Bone Miner Res 2001;16:992–1003. [PubMed: 11393796]
72. Ramasamy JG, Akkus O. Local variations in the micro-mechanical properties of mouse femur: the involvement of collagen fiber orientation and mineralization. J Biomech 2007;40:910–918. [PubMed: 16678186]
73. Tommasini SM, Nasser P, Schaffler MB, Jepsen KJ. Relationship between bone morphology and bone quality in male tibias: implications for stress fracture risk. J Bone Miner Res 2005;20:1372–1380. [PubMed: 16007335]
74. Keller TS, Mao Z, Spengler DM. Young's modulus, bending strength, and tissue physical properties of human compact bone. J Orthop Res 1990;8:592–603. [PubMed: 2355299]
75. Currey JD. Mechanical properties of mollusc shell. Symp Soc Exp Biol 1980;34:75–97. [PubMed: 7256572]
76. Bonfield W, Clark EA. Elastic deformation of compact bone. J Mater Sci 1973;8:1590–1594.
77. Tommasini SM, Nasser P, Jepsen KJ. Sexual dimorphism affects tibia size and shape but not tissue-level mechanical properties. Bone 2007;40:498–505. [PubMed: 17035111]
78. Harvey KB, Drummer TD, Donahue SW. The tensile strength of black bear (*Ursus americanus*) cortical bone is not compromised with aging despite annual periods of hibernation. J Biomech 2005;38:2143–2150. [PubMed: 16115638]
79. Harvey KB, Donahue SW. Bending properties, porosity, and ash fraction of black bear (*Ursus americanus*) cortical bone are not compromised with aging despite annual periods of disuse. J Biomech 2004;37:1513–1520. [PubMed: 15336926]

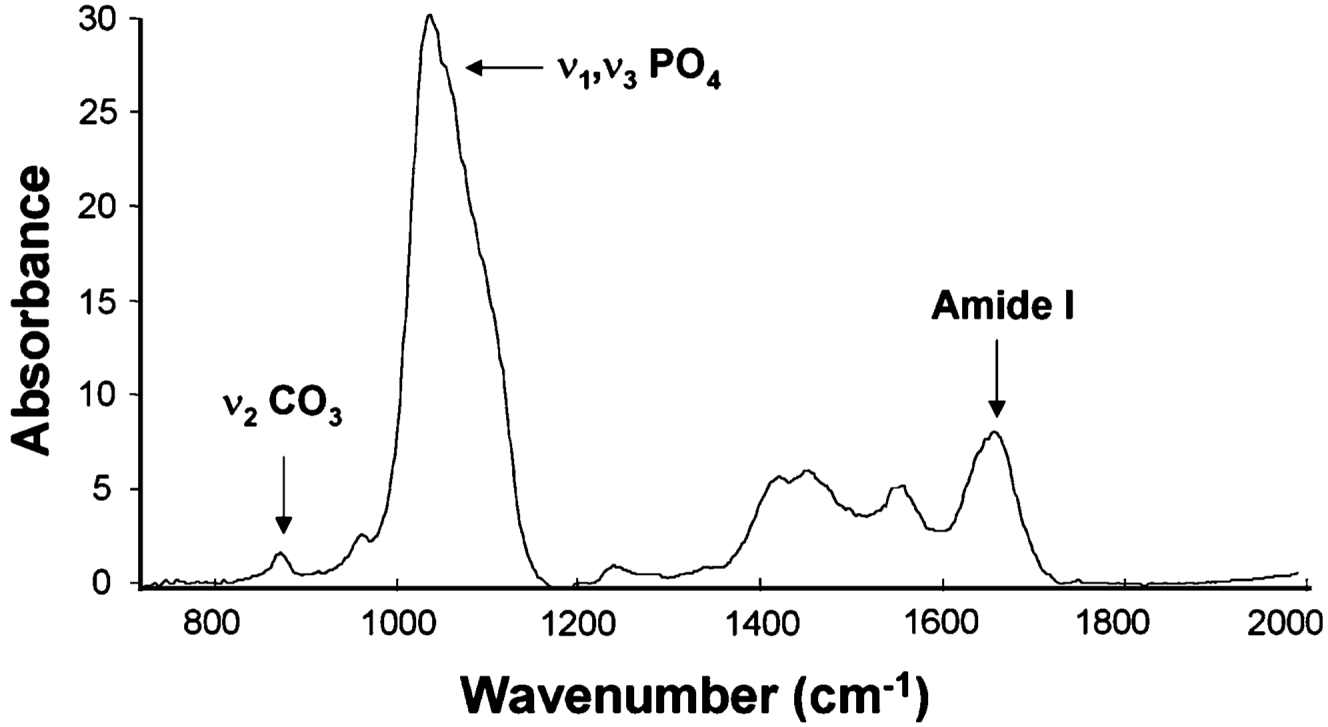

Fig. 1.
Representative FTIR spectrum for mouse femoral cortical bone from a B6 mouse with frequencies of interest labeled

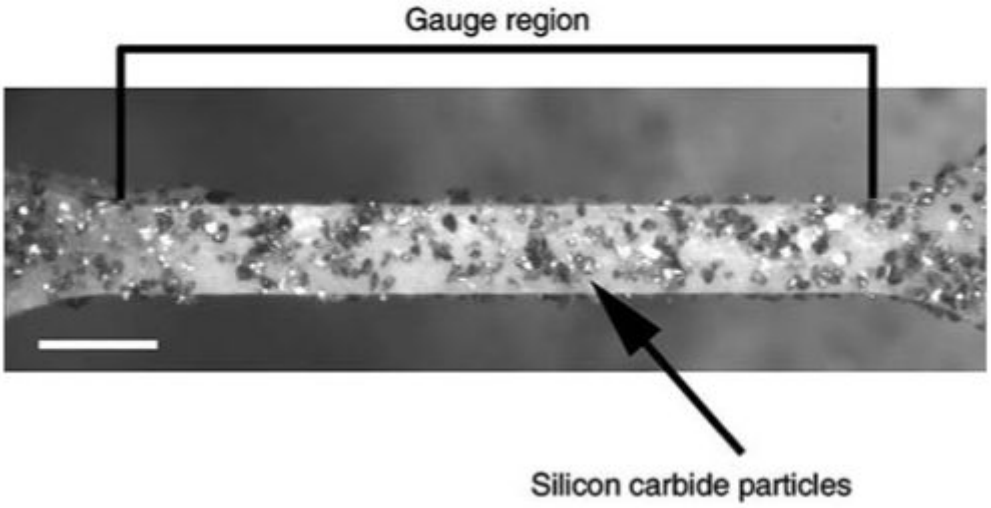

Fig. 2.
Representative mouse femora after milling to create a 280 μm wide × 3 mm long gauge region. Silicon carbide circles line the specimen and were used for subsequent strain calculations. Bar = 50 μm

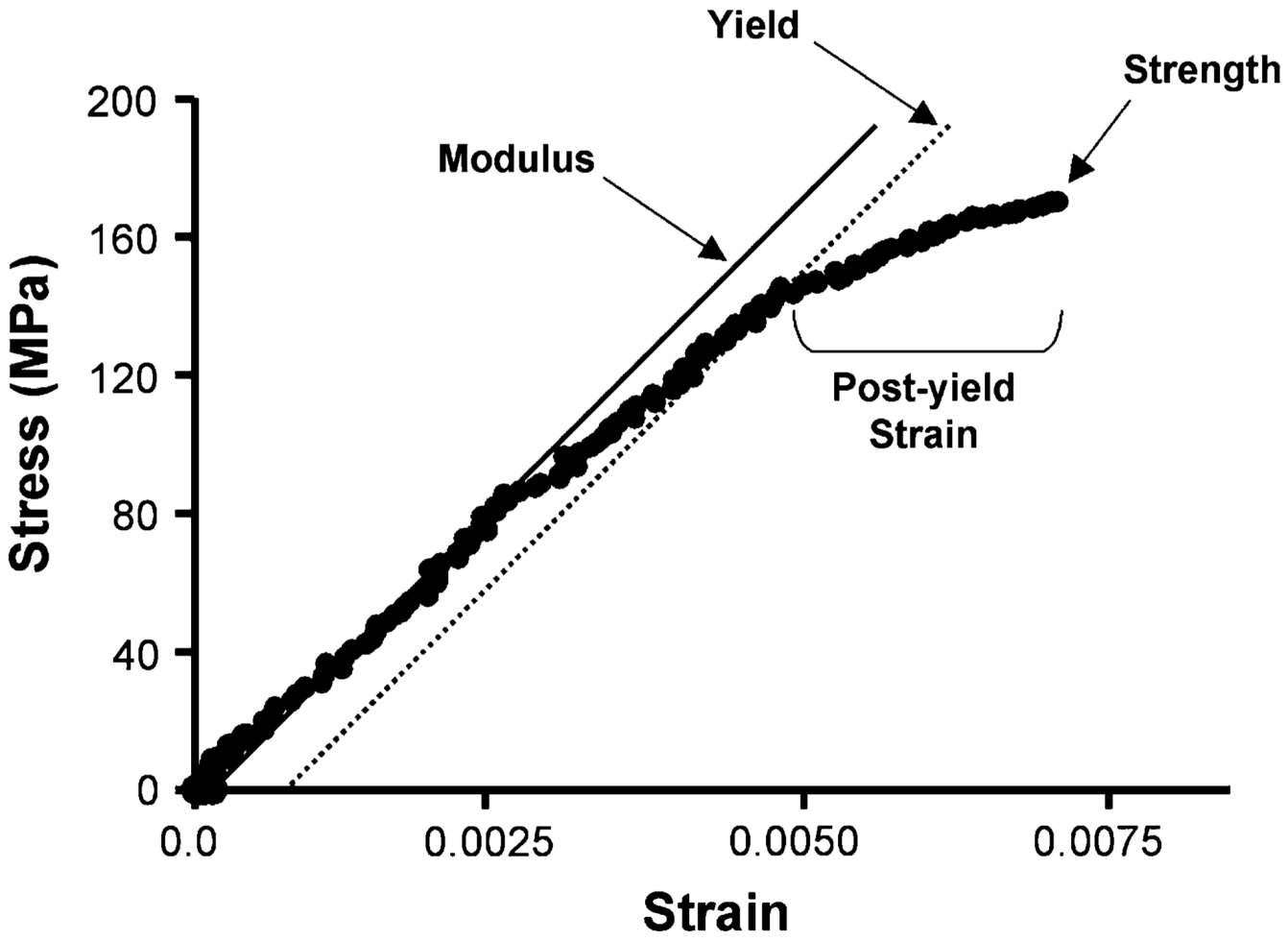

Fig. 3.

Representative stress/strain curve for a milled mouse femora. Modulus (E) was taken as the linear portion of the curve (before yield), strength as the maximum force before failure, post-yield strain as the deformation after yield, and work-to-failure as the area under the curve

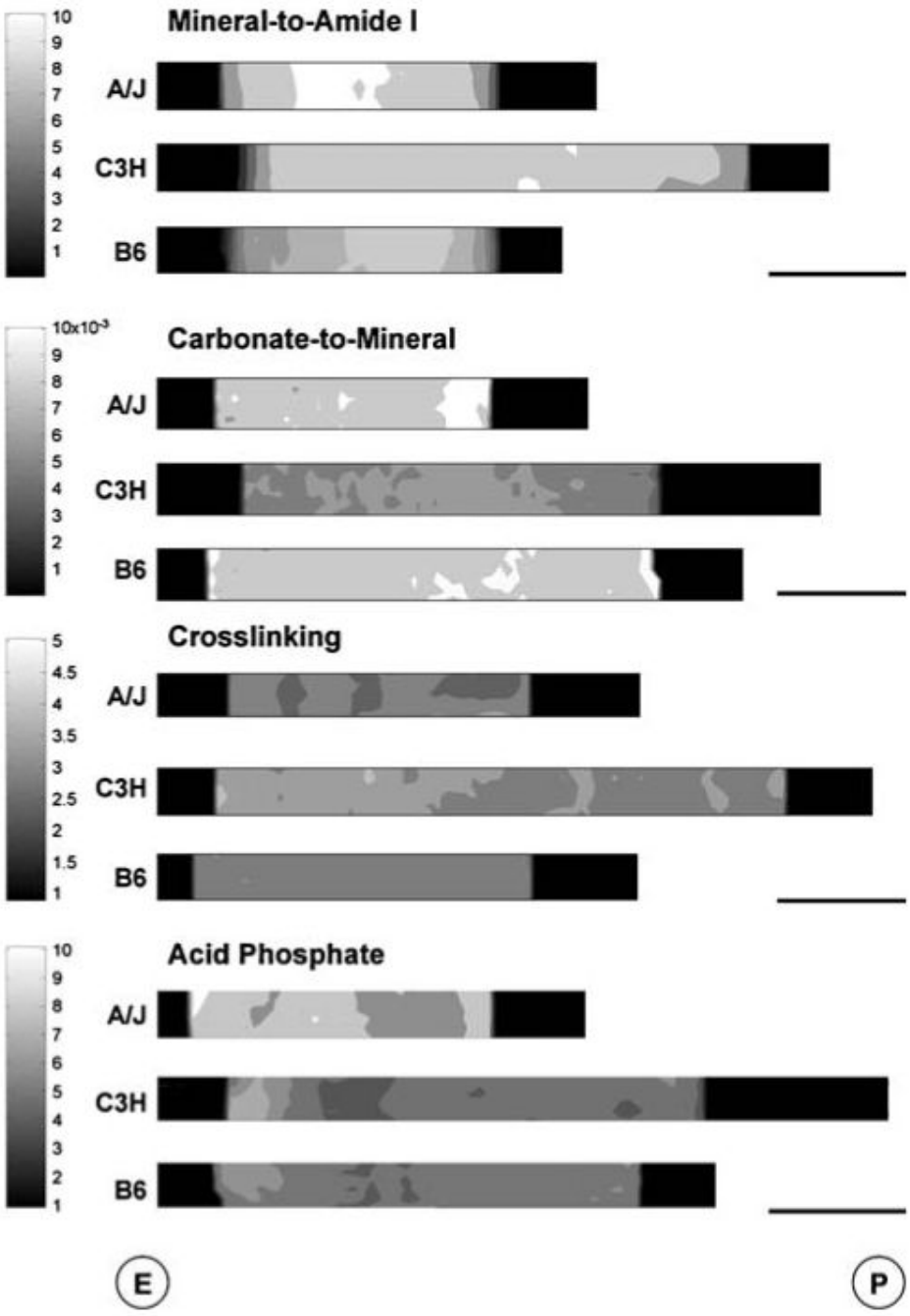

Fig. 4.

FTIR images showing representative spatial variation of spectral parameters among A/J, C3H, and B6 medial femoral cortices. Parameters shown are those for which at least one significant difference in mean trait values was found. Bar = 100 μm. E, endosteal surface; P, periosteal surface

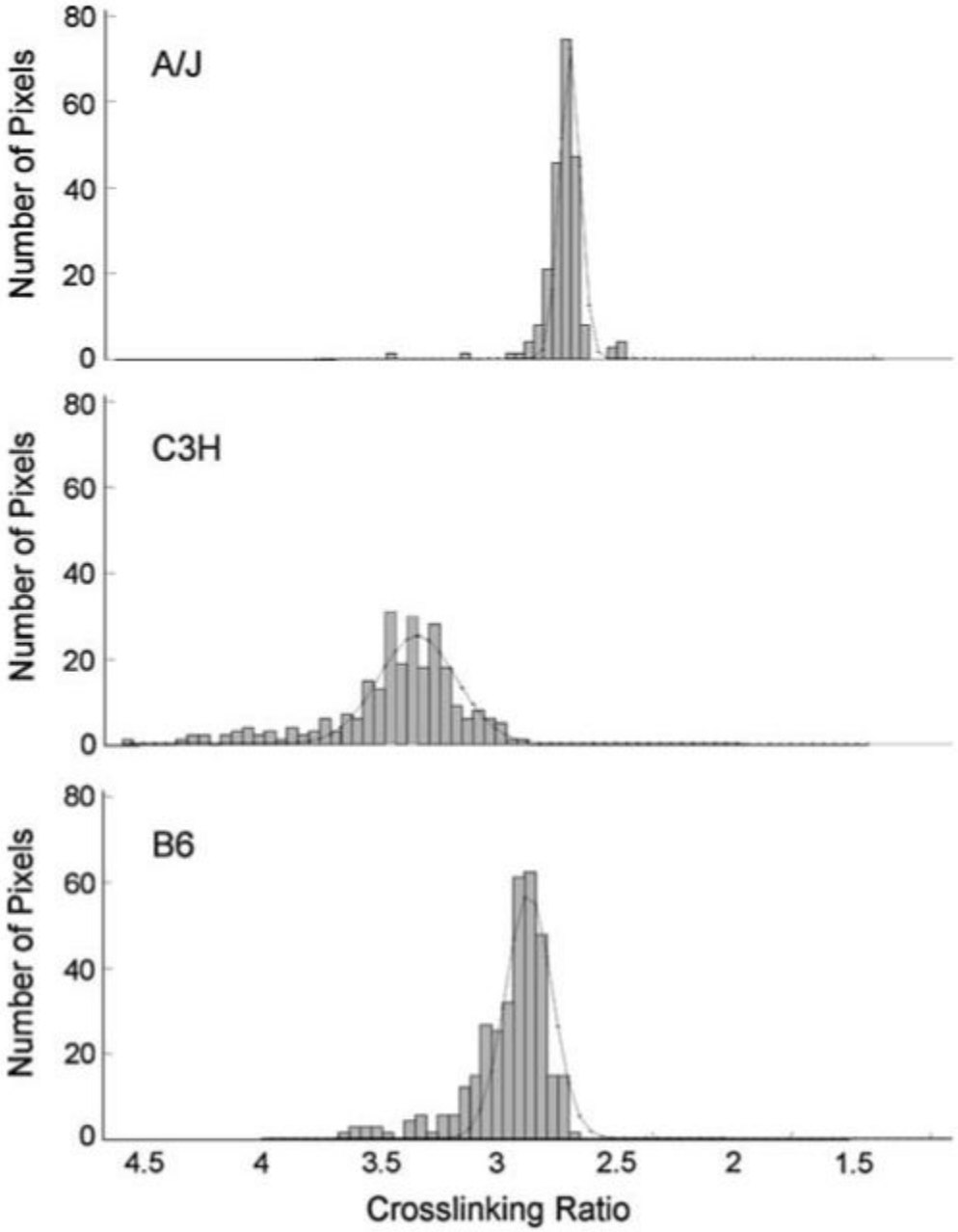

Fig. 5.

Representative pixel population histograms for collagen cross-linking. The curves represent Gaussian fits to the histogram used to calculate pixel distribution relative to the maximum. Note the wider curve at half-maximum for C3H

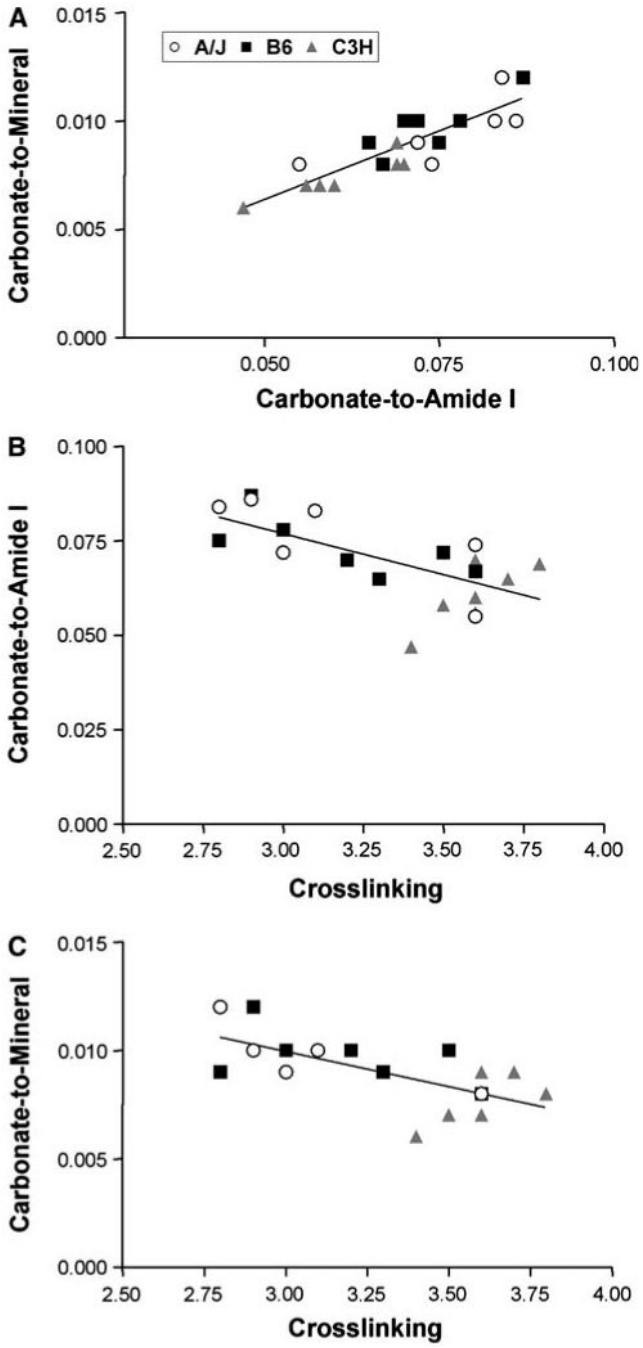

Fig. 6.

Correlations between FTIRI spectral parameters for A/J, B6, and C3H femora. Plots represent relationships with significant Pearson correlation coefficients ($R \geq 0.68$, $P < 0.05$) for data pooled across strains

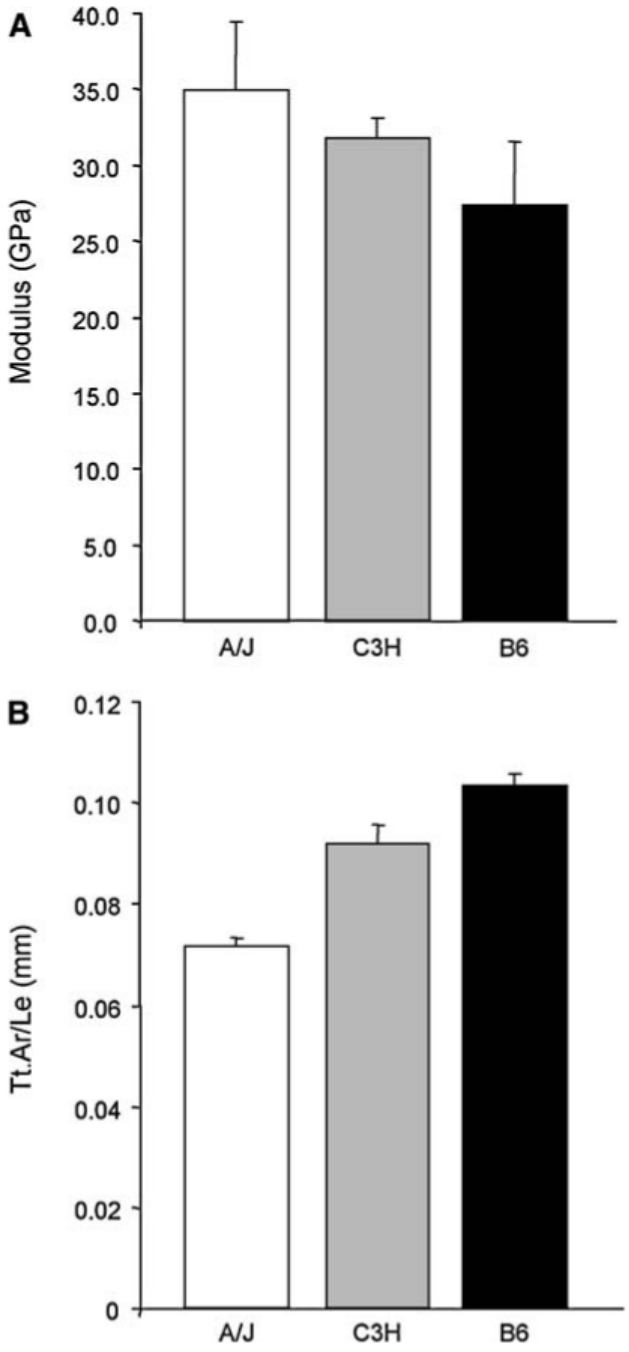

Fig. 7.

Plots for (**a**) mean modulus value and (**b**) Tt.Ar/Le for A/J, C3H, and B6 femora. Data are taken from Table 2 and illustrate the intraspecies trend of increased modulus with increased slenderness (decreased Tt.Ar/Le)

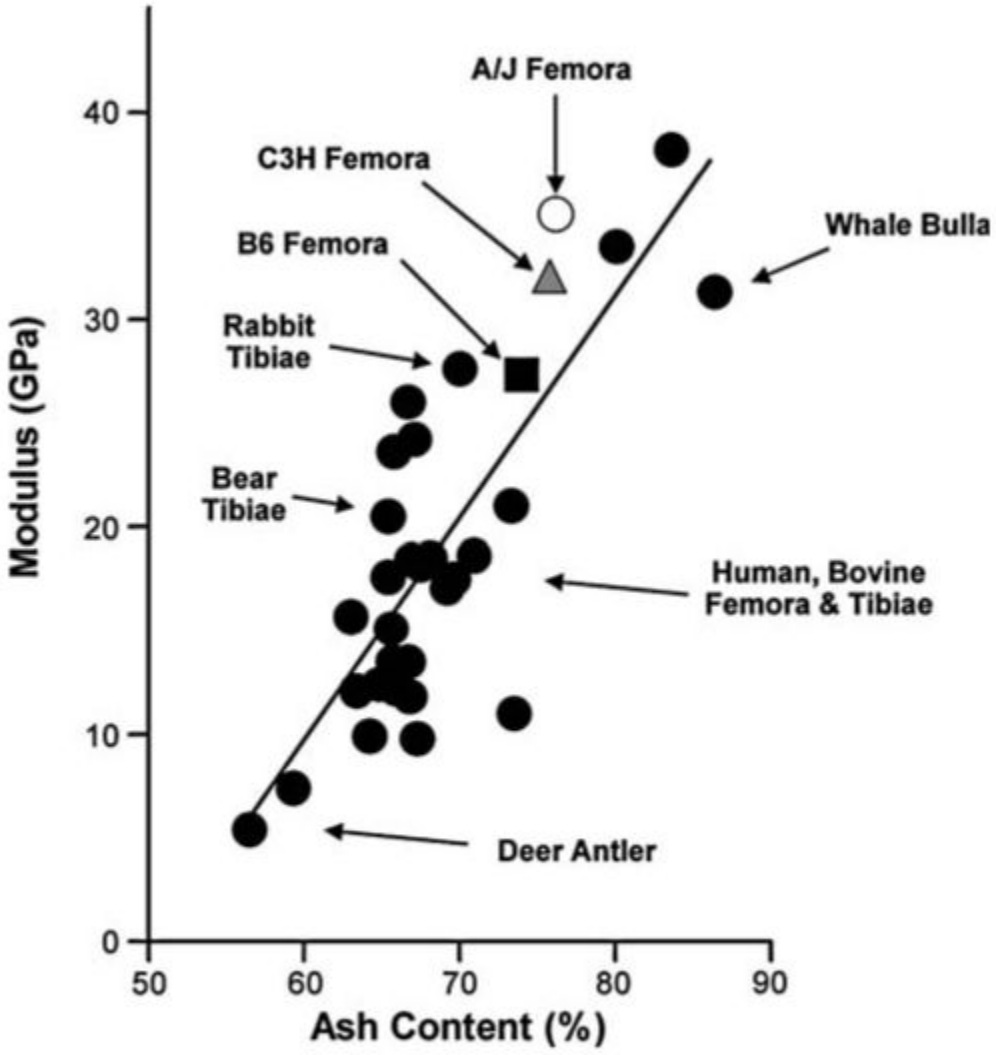

Fig. 8.
Modulus versus ash content (dry %) for a variety of animal bones [4,16,18,20,74-79]. R^2 = 0.65

Table 1

Mean values ± standard deviations for FTIRI spectral parameters and ash content from A/J, C3H, and B6 femora

	A/J	C3H	B6
Ash content (wet %)[a]	68.5 ± 1.0[†,‡]	67.4 ± 1.1[*,†]	65.1 ± 1.1[*,‡]
Mineral-to-amide I	8.4 ± 0.7[†]	8.0 ± 0.4	7.5 ± 0.4[*]
Carbonate-to-amide I	0.076 ± 0.012[‡]	0.062 ± 0.008[*]	0.074 ± 0.008
Carbonate-to-mineral	0.009 ± 0.002[‡]	0.008 ± 0.001[*,†]	0.010 ± 0.001[‡]
XLR (collagen cross-link ratio)	3.2 ± 0.3[‡]	3.6 ± 0.1[*,†,#]	3.2 ± 0.3[‡]
Crystallinity	1.198 ± 0.045	1.171 ± 0.038	1.188 ± 0.043
Acid phosphate	7.0 ± 1.1[‡]	5.5 ± 0.4[*]	6.6 ± 1.3

[a] Ash content (wet %) values as published previously [2]

[*] Significantly different from A/J, ANOVA $P < 0.05$

[†] Significantly different from B6, ANOVA $P < 0.05$

[‡] Significantly different from C3H, ANOVA $P < 0.05$

[#] Significantly different from A/J and B6 in pixel distribution, ANOVA $P < 0.05$

Table 2

Mean values ± standard deviations for tissue-level mechanical properties from A/J, C3H, and B6 femora

	A/J	C3H	B6
Modulus (GPa)	34.9 ± 4.4†	31.8 ± 1.4	27.4 ± 4.1*
Strength (MPa)	143.0 ± 25.8	164.0 ± 34.3	150.2 ± 23.6
Post-yield strain	0.001 ± 0.001	0.003 ± 0.002	0.003 ± 0.003
Total strain	0.005 ± 0.002	0.007 ± 0.003	0.012 ± 0.016
Work (MPa)	0.80 ± 0.49†	1.15 ± 0.71	1.50 ± 0.71*

*Significantly different from A/J, ANOVA $P < 0.05$

†Significantly different from B6, ANOVA $P < 0.05$